

# Solving the Coagulation Equation by the Moments Method

P. R. Estrada

*SETI Institute, 515 N. Whisman Rd., Mountain View, CA 94043*

and

J. N. Cuzzi

*NASA Ames Research Center, MS 245-3, Moffett Field, CA 94035*

## ABSTRACT

We demonstrate an approach to solving the coagulation equation that involves using a finite number of moments of the particle size distribution. This approach is particularly useful when only general properties of the distribution, and their time evolution, are needed. The numerical solution to the integro-differential Smoluchowski coagulation equation at every time step, for every particle size, and at every spatial location is computationally expensive, and serves as the primary bottleneck in running evolutionary models over long periods of time. The advantage of using the moments method comes in the computational time savings gained from only tracking the time rate of change of the moments, as opposed to tracking the entire mass histogram which can contain hundreds or thousands of bins depending on the desired accuracy. The collision kernels of the coagulation equation contain all the necessary information about particle relative velocities, cross-sections, and sticking coefficients. We show how arbitrary collision kernels may be treated. We discuss particle relative velocities in both turbulent and non-turbulent regimes. We present examples of this approach that utilize different collision kernels and find good agreement between the moment solutions and the moments as calculated from direct integration of the coagulation equation. As practical applications, we demonstrate how the moments method can be used to track the evolving opacity, and also indicate how one may incorporate porous particles.

*Subject headings:* accretion, accretion disks — methods: numerical — radiative transfer — solar system: formation

## 1. Introduction

The conditions under which planetary formation is initiated in the protoplanetary disk remain poorly understood despite several decades of astrophysical research. Furthermore, the continued discovery of extrasolar planets (over two hundred currently) further emphasizes the need to understand the formation of not only our own solar system, but of these numerous strange and diverse systems as well. At the forefront still remains the basic question of how growth occurs from dust to planet. The key properties of protoplanetary nebulae remain controversial, yet grain growth from dust to larger agglomerates ( $\sim$  cm-m), and from planetesimals ( $\gtrsim$  km) to planets must have occurred in some manner. While numerous studies of  $N$ -body dynamics have addressed the growth of terrestrial planets from asteroid-size planetesimals which are largely decoupled from the gas (e.g., Leinhardt & Richardson 2005; Bromley & Kenyon 2006), it is the transition from agglomerates to planetesimals which continues to provide the major stumbling block in planetary origins (Weidenschilling 1997, 2002, 2004; Weidenschilling & Cuzzi 1993; Stepinski & Valageas 1997; Dullemond & Dominik 2005; Cuzzi & Weidenschilling 2006; Dominik et al. 2007).

Grain growth begins with sticking of sub-micron sized grains, which are dynamically coupled to the nebula gas and collide at low relative velocities which are size-dependent (Weidenschilling & Cuzzi 1993). These relative velocities can be caused by a variety of mechanisms, such as Brownian motion for the smallest grains, differences in coupling to eddies in a turbulent nebula (Völk et al. 1980; Weidenschilling 1984; Markiewicz et al. 1991; Weidenschilling & Cuzzi 1993; Cuzzi & Hogan 2003; Ormel & Cuzzi 2007), and/or vertical, radial, and azimuthal drift driven by global gas pressure gradients (Nakagawa et al. 1986; Weidenschilling 1997). For the smallest sized grains and aggregates, sticking is caused by weak van der Waals interaction forces (although stronger forces may also act; see, e.g., Dominik et al. 2007). This sticking forms larger and larger aggregates until particles grow large enough to decouple from the gas and settle to the midplane where they may, barring strong turbulence (although see Johansen et al. 2007, for an exception), grow into larger objects, even planetesimals (Safronov 1969; Weidenschilling & Cuzzi 1993; Cuzzi et al. 1993; Weidenschilling 1997).

There is considerable observational evidence supporting dust growth in protoplanetary disks, at least from sub-micron to millimeter scales, based on observations of the dust continuum emission originating from protoplanetary disks. The wavelength dependence of dust emission from IR to radio wavelengths suggests, in many cases, that typical grain sizes are in the millimeter range, which is orders of magnitude larger than interstellar grains (Beckwith & Sargent 1991; Dullemond & Dominik 2005; Dominik et al. 2007). Measurements of the contrast of the Orion trapezium silicate emission feature at  $10 \mu\text{m}$  relative to the

local continuum implies an increase in size from interstellar dust (sub-micron) to micron sizes in the disk photospheres (van Boekel et al. 2003; Przygodda et al. 2003; Kessler-Silacci et al. 2006).

Theoretical approaches to the study of dust coagulation normally involve solving the cumbersome collisional coagulation equation (see Eq. 1) at each spatial location  $(R, \phi, Z)$  in the disk. The collisional kernel  $K(m, m')$  for particles of mass  $m$  and  $m'$  usually involves some sort of sticking efficiency, and particle cross-sectional area, in addition to the particle-particle relative velocities. Although the *systematic* particle-particle velocities that arise from gas pressure gradients (Nakagawa et al. 1986) are somewhat easy to incorporate into the collisional kernel, relative velocities in turbulence are more complicated. If one assumes that nebula turbulence follows a Kolmogorov inertial range (Völk et al. 1980) in which energy cascades from the largest, slowly rotating eddies, down to some minimum lengthscale where the intrinsic molecular viscosity can dissipate the macroscopic gas motions (and turbulence ceases), one can obtain closed-form expressions for the particle-particle, and particle-gas turbulent relative velocities (Cuzzi & Hogan 2003), even for particles of different sizes (Ormel & Cuzzi 2007). Numerical models of particle growth in the inner regions of protoplanetary disks indicate that inclusion of these turbulence-induced relative velocities is essential (Dullemond & Dominik 2005), as it provides a source of energetic collisions that, in the presence of fragmentation and destruction, leads to the ongoing existence of small grains even after several million years.

A full scale solution to the problem of dust coagulation for a size spectrum at every vertical and radial location in the protoplanetary disk, as a function of time, is thus prohibitive even with today’s computational capabilities (Weidenschilling 2002, 2004). So it is advantageous to find alternative methods of extracting information from the coagulation process, such as time scales of growth, the largest particle size, the size that dominates the area (radiative transfer), and the size that dominates the mass (migration and redistribution) without having to track the behavior of the entire mass distribution.

In this paper, we describe a method that utilizes the moments of the coagulation equation to accomplish this task, in particular when the functional form of the mass distribution can be assumed. In § 2, we derive the moment equations from the coagulation equation, and compare direct integration of the coagulation equation with solutions using the moments approach in the case of a simple turbulent coagulation kernel. We also present two different approaches to obtaining solutions using a realistic kernel, when the form of the size distribution is assumed to be a powerlaw. In § 3, we evaluate the different approaches developed in § 2 for realistic kernels by numerical integration of the moments equations and compare these moments to those obtained by direct integration of the coagulation equation. We also

compare the moments solution to an alternate analytical approach by Garaud (2007). In § 4, as a demonstration of the practical application of the moments method, we calculate the wavelength-independent opacity, and discuss generalization to wavelength-dependent Planck or Rosseland mean opacities. In § 5, we indicate how porosity may be included. In § 6, we present our conclusions.

## 2. Solution Techniques Using the Moments Method

The moments method approach to modeling particle growth allows an attractive alternative to solving the full coagulation equation when it is only necessary to know a particular property, or properties of the evolving particle size distribution. The coagulation equation (Smoluchowski 1916) in its integro-differential form is given by

$$\frac{df(m, t)}{dt} = \frac{1}{2} \int_0^m K(m - m', m') f(m - m', t) f(m', t) dm' - \int_0^\infty K(m, m') f(m, t) f(m', t) dm' + \left. \frac{df}{dt} \right|_+ + \left. \frac{df}{dt} \right|_-, \quad (1)$$

where  $f(m, t)$  is the particle number density per unit mass at mass  $m$ , and  $K(m, m')$  is the collision kernel connecting the properties of interacting masses  $m$  and  $m'$ , which typically takes into account mutual particle cross section  $\sigma(m, m')$ , relative velocity  $\Delta V(m, m')$ , and a particle sticking efficiency  $S(m, m')$ . The last two terms on the RHS of Eq. (1) represent sources and sinks such as particle erosion, fragmentation and subsequent redistribution of the fragmented population, and gravitational growth. Although we will not specifically address these mechanisms, we will indicate how they may be treated, and save implementation for a forthcoming paper.

The motivation behind using the moments method is to avoid the computational cost inherent in Eq. (1) which entails solving the convolution integral (the first term on the RHS of Eq. 1) at every location, and at every time step. Depending on the functional form of the kernel, the second integral on the RHS may also need to be integrated repeatedly. Given that the typical mass spectrum may involve  $10^2 - 10^3$  bins to acquire the desired accuracy, the computational burden required becomes a detriment to any study involving a wide range of parameter space. The so-called brute force solution of the coagulation equation thus becomes the primary bottleneck in running 2D evolutionary models over extended periods of time (Weidenschilling 2004; Dullemond & Dominik 2005).

We define the  $p$ -th moment  $M_p$  of the distribution, where  $p$  need not be an integer, as

$$M_p = \int_0^\infty m^p f(m, t) dm, \quad (2)$$

where the units of  $f(m, t)$  are such that  $M_0 = \int f(m, t) dm$  represents the total number density of particles, and  $M_1 = \int m f(m, t) dm = \rho$  is the total volume mass density of solids. The essence of the moments method is as follows. We multiply both sides of the coagulation equation (Eq. 1) by  $m^k$ , where  $k$  is an integer, and then integrate both sides over mass  $m$ :

$$\begin{aligned} \frac{dM_k}{dt} = \int_0^\infty m^k \frac{df}{dt} dm = \frac{1}{2} \int_0^\infty m^k dm \int_0^m K(m - m', m') f(m - m', t) f(m', t) dm' - \\ \int_0^\infty m^k f(m, t) dm \int_0^\infty K(m, m') f(m', t) dm'. \end{aligned} \quad (3)$$

We introduce a step function  $H(m - m')$ , such that  $H = 0$  for  $m - m' < 0$  and  $H = 1$  otherwise, to extend the limits of the integral over  $m'$  from  $(0, m)$  to  $(0, \infty)$ . The convolution integral (the first integral on the RHS of Eq. 3) then becomes

$$\begin{aligned} \frac{1}{2} \int_0^\infty m^k dm \int_0^\infty H(m - m') K(m - m', m') f(m - m', t) f(m', t) dm' = \\ \frac{1}{2} \int_0^\infty f(m', t) dm' \int_0^\infty (u + m')^k K(u, m') f(u, t) du, \end{aligned} \quad (4)$$

where on the RHS of Eq. (4) we have switched the order of integration and made the substitution  $u = m - m'$ . The RHS side of Eq. (4) may then be combined with the last double integral in Eq. (3) to yield the set of ordinary differential equations (ODEs) for the integer moments (Marov & Kolesnichenko 2001):

$$\frac{dM_k}{dt} = \int_0^\infty \int_0^\infty \left[ \frac{1}{2} (m + m')^k - m^k \right] K(m, m') f(m, t) f(m', t) dm dm', \quad (5)$$

where we have substituted  $m$  for  $u$  with no loss of generality. Depending on the mass dependence of the kernel (as illustrated below) the right hand side can readily be expressed as products of moments of order  $k$  or less, leading to a closed system of equations which may be solved using standard techniques. In this definition of the coagulation equation in which it is assumed there are no sources and sinks, the first moment  $M_1 \equiv \rho$  is constant in time,

that is  $dM_1/dt = 0$ <sup>1</sup>.

Exact solutions to the coagulation equation have been obtained for some specific choices of the kernel (e.g., Smoluchowski 1916; Trubnikov 1971), the most simple being that of constant kernel  $K(m, m') = \beta_0$ . Although the exact solution for  $f(m, t)$  cannot be obtained from the moments equations, the time rate of change of the zeroth moment ( $k = 0$ ), can easily be obtained from Eq. (5) which reduces to  $dM_0/dt = -(1/2)\beta_0 M_0^2$  and has the trivial solution (see, e.g., Silk & Takahashi 1979)

$$M_0(t) = \frac{M_0(0)}{1 + (1/2)\beta_0 M_0(0)t}, \quad (6)$$

independent of the initial choice of distribution  $f(m, 0)$ . Likewise, the ODE for  $M_2$ , which can be associated with the density-weighted mean particle size ( $\langle m \rangle = M_2/M_1$ ), yields the simple solution  $M_2(t) = M_2(0) + \beta_0 \rho^2 t$ . Despite not knowing the exact solution, we are able to understand the behavior of general properties of the mass distribution with time through the moments equation without tracking the behavior of the full mass spectrum. Thus, if it is only desired to know, for example, the time evolution of the particle representing most of the *area* (first moment) or most of the *mass* (second moment) of the distribution, then the advantage of the moments method becomes clear. A small number of moments is all that is necessary to determine the behavior of the system. In particular, we will be interested in the size of the largest particle  $m_L(t)$  in the entire mass distribution as a function of time (which we show below can be computed from the integer moments), because these are usually the most rapidly drifting and most violently colliding particles (Cuzzi & Weidenschilling 2006).

### 2.1. Example: Saffman and Turner Turbulent Coagulation Kernel

We can illustrate the moments method approach using a very simple turbulent coagulation kernel where  $K(m, m') = \gamma_0(m^{1/3} + m'^{1/3})^3$  (Saffman & Turner 1956), and no sources or sinks. Physically, this represents the product of  $(r + r')^2$  for area, and  $(r + r')$  for relative velocity of two particles in a laminar shear flowfield. If a sticking coefficient were desired then we would specifically have  $K(m, m') = \gamma_0(m^{1/3} + m'^{1/3})^3 S(m, m')$  where  $0 \leq S(m, m') \leq 1$ . Here,  $\gamma_0$  is a constant that depends on the Reynolds number of the gas flow. Inserting this kernel into Eq. (5), we find the set of equations

---

<sup>1</sup>We note that under realistic protoplanetary nebula conditions,  $\rho$  will not be constant due to, e.g., size-dependent advection terms in the equations. Such effects can be treated separately from the “coagulation” step. See § 2.2.2.

$$\begin{aligned} \frac{dM_0}{dt} &= -\gamma_0(M_0M_1 + 3M_{1/3}M_{2/3}), & \frac{dM_1}{dt} &= 0 \\ \frac{dM_2}{dt} &= 2\gamma_0(M_2M_1 + 3M_{4/3}M_{5/3}). \end{aligned} \quad (7)$$

We note that the physical derivation of kernels in terms of particle radius  $r$  leads to *fractional* moments in terms of  $m$ . These fractional moments look complicated, but can be solved for by simple interpolation using Lagrange polynomials in terms of the more familiar integer moments (Loginov 1979; Press et al. 1992; Marov & Kolesnichenko 2001). Thus, any fractional moment  $M_p$  may be expressed compactly in the normalized form  $M'_p(t) = M_p(t)/M_p(0)$ :

$$M'_p(t) = \prod_{j=k}^{k+n} [M'_j(t)]^{L_j^n(p)}, \quad (8)$$

where  $n$  is the number of integer moments,  $k = 0, 1, \dots, n$ , and the exponent  $L_j^n$  is defined as

$$L_j^n(p) = \frac{1}{n!} \prod_{n+1} (p) \frac{(-1)^{n-j} C_n^j}{p-j}, \quad (9)$$

with  $\prod_{n+1}(p) = p(p-1)\dots(p-n)$ , and the  $C_n^j$  are the binomial coefficients  $n!/j!(n-j)!$ . The important thing to note here is that the order of the moments must remain less than or equal to the largest moment in order for the system to remain closed. In general, this will be true for realistic collision kernels (see § 2.2).

To test the accuracy of the moments method, we integrated equations (7) using a fourth order Runge-Kutta scheme, and compared the results to a brute force integration of the coagulation equation (Eq. 1). For the latter, we integrated the distribution function  $f(m, t)$  at each timestep to determine the moments of the distribution  $M_0$ ,  $M_1$ , and  $M_2$ . We chose  $f(m, 0) = c_0 m^{-q}$  as our initial distribution for simplicity. Since the form of the mass distribution is only assumed at  $t = 0$ , we consider this to be an example of an implicit assumption (see § 2.2.2). The results of this calculation are presented in Figure 1. We have used two different resolutions for the brute force calculation in order to demonstrate how the higher resolution (and much more computationally expensive) case (solid symbols) approaches the moments approach solution. Notice that the first moment  $M_1 = \rho$  remains constant as expected. Given that general numerical errors can arise from the finite mass grid and coarse timesteps ( $\Delta t = 10$  years) used for the calculation, and that systematic errors may be introduced by the Lagrangian interpolation, the fit is quite good. It is important to point out here that while the coagulation calculation required as many as 20 – 30 hours of CPU

time to complete on a 2 GHz machine, the moments calculation of Eq. (7) is essentially instantaneous.

## 2.2. Realistic Coagulation Kernels

The Saffman-Turner turbulent coagulation kernel we used as an example in § 2.1 is simple to utilize and is expressible explicitly in powers of the mass  $m$ . In practice, however, the realistic coagulation kernels that we will be using will be more complicated than this simple example. A realistic coagulation kernel will be, at the very least, a product of a mutual cross section  $\pi(r + r')^2$  and a relative velocity

$$\Delta V(m, m') = \sqrt{(U - U')^2 + (V - V')^2 + (W - W')^2 + v_T^2(m, m')}, \quad (10)$$

where  $U(m)$ ,  $V(m)$ , and  $W(m)$  are the  $x, y, z$  systematic (pressure gradient driven) particle velocities, and  $v_T$  is the turbulent velocity contribution which in general is not separable into distinct functions of  $m$  and  $m'$  (Cuzzi & Hogan 2003; Ormel & Cuzzi 2007). The systematic velocities, which are derived for a discretized particle size distribution in the appendix, are complicated functions of the particle size through the stopping time  $t_s$ ,

$$t_s = \frac{m \Delta V_{pg}}{F_D}, \quad (11)$$

where  $\Delta V_{pg} = |\vec{\mathbf{V}} - \vec{\mathbf{v}}|$  is the relative velocity between the particle and the gas, and  $F_D$  is the drag force on the particle of size  $r$  which depends on the size of the particle relative to the mean free path  $\lambda$  of the gas molecule (e.g., see Cuzzi et al. 1993). Depending on whether  $r \gtrsim \lambda$  or  $r \lesssim \lambda$  determines whether the stopping time itself depends on the instantaneous relative velocity  $\Delta V_{pg}$  between the particle and the gas (Stokes regime) or does not (Epstein regime). In the latter case, calculation of the systematic velocities ( $U, V, W$ ) and gas velocities ( $u, v, w$ ) for a particle size distribution is straightforward. In the former case, iterations are required to correctly calculate  $\Delta V_{pg}$  (see appendix).

The turbulent velocities are less straightforward to implement than their systematic counterparts because of the different coupling that exists between particles and eddies of different sizes (and thus stopping and decay times, respectively). It has not been until very recently that closed form expressions for the turbulence-induced velocities (for a particle size distribution) were derived (Ormel & Cuzzi 2007). These expressions can be written



separately for the so-called “class I” and “class II” eddies<sup>2</sup> as:

$$\Delta V_I^2 = v_g^2 \frac{\text{St}_i - \text{St}_j}{\text{St}_i + \text{St}_j} \left( \frac{\text{St}_i^2}{\text{St}_{ij}^* + \text{St}_i} - \frac{\text{St}_i^2}{1 + \text{St}_i} - \frac{\text{St}_j^2}{\text{St}_{ij}^* + \text{St}_j} + \frac{\text{St}_j^2}{1 + \text{St}_j} \right), \quad (12)$$

$$\Delta V_{II}^2 = v_g^2 \left( 2(\text{St}_{ij}^* - \text{Re}^{-1/2}) + \frac{\text{St}_i^2}{\text{St}_i + \text{St}_{ij}^*} - \frac{\text{St}_i^2}{\text{St}_i + \text{Re}^{-1/2}} + \frac{\text{St}_j^2}{\text{St}_j + \text{St}_{ij}^*} - \frac{\text{St}_j^2}{\text{St}_j + \text{Re}^{-1/2}} \right), \quad (13)$$

where  $v_T^2 = \Delta V_I^2 + \Delta V_{II}^2$ ,  $\text{Re}$  is the Reynolds number,  $v_g = \alpha^{1/2} c_g$  is the turbulent gas velocity with  $c_g$  the sound speed (e.g., Nakagawa et al. 1986; Cuzzi & Weidenschilling 2006), and the particle Stokes numbers  $\text{St}_i = t_{si}/t_L$ , where  $t_L$  is the turnover time of the largest eddy, typically taken to be  $\Omega^{-1}$ . The boundary between class I and class II is defined by the “combined” Stokes number  $\text{St}_{ij}^* = \max(\text{St}_i^*, \text{St}_j^*)$  and the values of the  $\text{St}_k^*$  are obtained from the equation (Ormel & Cuzzi 2007):

$$\frac{2}{3} y_k^* (y_k^* - 1)^2 - \frac{1}{1 + y_k^*} = -\frac{\text{St}_k}{1 + \text{St}_k} + \frac{1}{\text{St}_k} \frac{\Delta V_{pg}^2}{v_g^2}, \quad (14)$$

where  $y_k^* = \text{St}_k^*/\text{St}_k$ . In our calculations, we will make use of these expressions when comparing cases with turbulence-induced velocities.

Given that the moments method requires that we express the kernel in terms of fractional or integer moments, the problem becomes expressing the relative velocity (Eq. 10) in a form that satisfies this requirement. As an example, the systematic velocities  $U$ ,  $V$ , and  $W$  can each be fit easily by a finite series in fractional powers  $p_i$  of  $m$  as  $U(m) = \sum_i^N a_i m^{p_i}$  where the coefficients  $a_i$  can be found by fitting  $N$  points to the function  $U(m_l) = U_l$  ( $l$  an integer). This leads to the system of equations

$$U_l = \sum_{i=1}^N a_i m_l^{p_i}. \quad (15)$$

---

<sup>2</sup>The concept of eddy classes were introduced by Völk et al. (1980) to distinguish between slowly and rapidly varying eddies. Class I eddies are defined as those in which the eddy fluctuates slowly enough that a particle’s stopping time  $t_s$  is much shorter than the eddy decay time and the time it takes to cross the eddy; thus, they will align themselves with the gas motions of the eddy prior to its decay. Class II eddies then are defined as ones in which the eddy decay time is fast compared to the particles  $t_s$ , and thus only provide a small perturbation to the particle motion.

The coefficients  $a_i$  then follow from matrix inversion. Similarly, one can find expressions  $V(m) = \sum_i^N b_i m^{p_i}$ , and  $W(m) = \sum_i^N c_i m^{p_i}$  so that we may construct the laminar expression for  $(\Delta V)^2$  in terms of the variables  $m$  and  $m'$  by multiplying out the individual terms, e.g.,  $U(m)U(m') = \sum_{i,j} a_i a_j m^{p_i} m'^{p_j}$  and so on. We find then that we can express the square of Eq. (10) as

$$(\Delta V(m, m'))^2 = \sum_{i,j} A_{ij} [m^{p_i+p_j} - 2m^{p_i} m'^{p_j} + m'^{p_i+p_j}], \quad (16)$$

where  $A_{ij} = a_i a_j + b_i b_j + c_i c_j$ , and  $p_i + p_j \leq 2$  for closure. This determines the matrix of coefficients  $A_{ij}$  which operate on the finite power series in  $m$  and  $m'$ . Although we cannot use the same approach for solving for  $\Delta V$  in Eq. (10) because of the radical, we were motivated to express  $\Delta V$  in a similar form, i.e., as  $\Delta V(m, m') = \sum_{i,j} A'_{ij} [m^{p_i+p_j} - 2m^{p_i} m'^{p_j} + m'^{p_i+p_j}]$ , and  $p_i + p_j \leq 1$ . The problem reduces to solving for the coefficients  $A'_{ij}$  directly, by similar matrix inversion techniques. Unfortunately, the number of points needed to obtain an accurate representation of the two-variable function  $\Delta V(m, m')$  this way exceeds the limitations of the inversion. In practice we found that we could solve a system for  $\Delta V$  with at most 5 – 6 points (25 – 36 matrix elements), whereas Eq. (16) carries much less restriction in the number of points needed because we could construct  $(\Delta V)^2$  by the product of accurate representations of single variable functions. Furthermore, due to the coupling evident in the turbulence induced velocities (Equations 12 and 13), the turbulent velocities are not separable functions of the masses  $m$  and  $m'$ , further complicating the analysis.

*Powerlaw assumption:* Fortunately, it turns out that, although the direct calculation approach to  $\Delta V$  described above would be mathematically appealing in the sense that the moment equations would remain implicit (i.e., the form of the mass distribution would only be assumed at  $t = 0$ ), it is not necessary. In the next sections we describe two alternative approaches to dealing with realistic coagulation kernels that employ the moments method under the assumption that the form of the mass distribution  $f(m, t)$  is a powerlaw. Such an assumption is not entirely unfounded. A number of detailed models by Weidenschilling (1997, 2000, 2004) have shown that powerlaw size distributions result, which have nearly constant mass per decade radius to an upper limit  $m_L(t)$  which grows with time until the frustration limit of around a meter is reached, and (under turbulent conditions, at least) growth stalls (Cuzzi & Weidenschilling 2006). Similar trends are found by Dullemond & Dominik (2005) in which different assumptions about collisional ejecta are made. These authors do find minor fluctuations in the distribution, but if one is primarily interested in general properties of the distribution, such as how the largest particle size changes with time, and not the fine structure of the mass distribution itself, the approach is quite advantageous. There are reasons to believe that a powerlaw is a natural end-state, especially those with equal mass

per decade, because they have self-preserving properties for the collision kernels of interest (Cuzzi & Weidenschilling 2006).

The significance of the upper mass cutoff  $m_L$  depends on the assumed slope of the powerlaw. In all real distributions, there will be a rapidly decreasing abundance of particles for masses exceeding some threshold, even though the abundance may not drop immediately to zero as in our assumed model. The rare, extremely large particles might be of interest for some applications, but our focus will be the particle size carrying most of the area, or most of the mass (the first or second moments). For powerlaw distributions  $f(m) \propto m^{-q}$  with  $q < 2$ ,  $m_L$  is itself the mass of the particle carrying most of the mass and is independent of the selection of a lower particle size cutoff. For  $q = 2$ , the distribution contains equal mass per decade, and for  $q > 2$ , most of the mass is in the small particles and the value of  $m_L$  depends on the lower particle size chosen. Most realistic distributions, and those most commonly treated in the literature, have  $q < 2$ ; here we assume  $q = 11/6$ , a widely used fragmentation powerlaw. In this case, a strict cutoff at  $m_L$  represents a well-defined distribution with easily-understood moments where most of the mass is at  $m_L$  and the area is nearly equally distributed per decade with a mass dependence  $m^{-1/6}$ .

Although we do not include either imperfect sticking or fragmentation at this stage in the model, we believe that the moment equations as expressed in Eq. (5) will remain valid up to a "fragmentation barrier", which may be defined as that size for which the typical disruption energy of a particle is on the same order as the energy of identical colliding particles. The fragmentation barrier will also depend on one's choice of nebula parameters. This treatment (up to the fragmentation size) is consistent with recent work by Brauer et al. (2008) (their Fig. 13) which shows a constant powerlaw mass distribution up to a cutoff size which then falls off abruptly. This "knee" in the distribution represents that efficient fragmentation size.

Once  $m_L$  reaches the fragmentation barrier, growth beyond this stage would need to be treated in a different manner, for example, by simple sweepup of small, less disruptive particles by large ones (Cuzzi et al. 1993). Creation and disruption of these particles can be handled as part of the source and sink terms in which for example, disrupted particles are assumed to be fragmented back into a powerlaw distribution (which is suggested by experimental evidence and widely assumed by other modelers) as opposed to monomers. The model as presented within this paper, however, should be useful for the early stages of protoplanetary nebula particle growth relevant to spectral energy distributions and MRI suppression. We leave the incorporation of growth stages beyond the efficient fragmentation stage for a later paper.

### 2.2.1. Approach 1: Explicit Assumption

Motivated by our discussion of the previous section, if we assume that the form of the particle mass distribution function remains a powerlaw at all times, we may express  $f(m, t) = c(t)m^{-q}$ , such that  $m_L(t)$  is the growing upper limit of the distribution,  $q$  is the slope which is assumed to be constant (although see below), and  $c(t)$  is a normalization coefficient. Taking the lower limit of the mass distribution to be  $m_0$ , then moments as expressed in Eq. (2) are explicitly given for  $q - p \neq 1$  by

$$M_p(t) = \frac{c(t)}{1 + p - q} (m_L(t)^{1+p-q} - m_0^{1+p-q}). \quad (17)$$

We then take the time derivative of Eq. (17) for the zeroth and second moments, and substitute these expressions on the LHS of the corresponding moment equations in Eq. (5) to get

$$\frac{m_L^{1-q} - m_0^{1-q}}{1 - q} \frac{dc}{dt} + cm_L^{-q} \frac{dm_L}{dt} = -\frac{1}{2} c^2 \Gamma_0(m_L), \quad (18)$$

$$\frac{m_L^{3-q} - m_0^{3-q}}{3 - q} \frac{dc}{dt} + cm_L^{2-q} \frac{dm_L}{dt} = c^2 \Gamma_2(m_L), \quad (19)$$

where Eq. (18) is valid for  $q \neq 1$ , and  $\Gamma_0$  and  $\Gamma_2$  are the integrals on the RHS of Eq. (5) for  $k = 0$  and  $k = 2$ , respectively. That is

$$\Gamma_0(m_L) = \int_{m_0}^{m_L(t)} \int_{m_0}^{m_L(t)} K(m, m') m^{-q} m'^{-q} dm dm', \quad (20)$$

$$\Gamma_2(m_L) = \int_{m_0}^{m_L(t)} \int_{m_0}^{m_L(t)} K(m, m') m^{1-q} m'^{1-q} dm dm', \quad (21)$$

where the kernel is given by  $K(m, m') = \sigma(m, m') \Delta V(m, m') S(m, m')$ , with  $\sigma(m, m') = K_0(m^{1/3} + m'^{1/3})^2$ ,  $K_0 = \pi(3/4\pi\rho_s)^{2/3}$ , and  $\rho_s$  is the particle material density, assumed constant. Note that for the special case of  $q = 1$ , Eq. (18) has a slightly different form which depends on  $\ln(m_L/m_0)$ . After some simple algebra, Eq.'s (18) and (19) can be written as

$$\frac{dm_L}{dt} = c \left[ \frac{(3 - q)(m_L^{1-q} - m_0^{1-q})\Gamma_2 + \frac{1}{2}(1 - q)(m_L^{2-q} - m_0^{2-q})\Gamma_0}{(3 - q)(m_L^{1-q} - m_0^{1-q})m_L^{2-q} - (1 - q)(m_L^{3-q} - m_0^{3-q})m_L^{-q}} \right], \quad (22)$$

$$\frac{dc}{dt} = -c^2 \left[ \frac{(3-q)(1-q)(m_L^{-q}\Gamma_2 + \frac{1}{2}m_L^{2-q}\Gamma_0)}{(3-q)(m_L^{1-q} - m_0^{1-q})m_L^{2-q} - (1-q)(m_L^{3-q} - m_0^{3-q})m_L^{-q}} \right], \quad (23)$$

which we integrate using a fourth order Runge-Kutta scheme. Equation (17) then gives the moments  $M_0$  and  $M_2$  as a function of time, which can be directly compared with direct integration of the same conditions using the coagulation equation (Eq. 1).

The advantage of this approach (in which a powerlaw is assumed at all times) is its transparency; that is, the variables being sought ( $m_L$  and  $c$ ) are solved for directly. Furthermore, the change in the coagulation kernel as the particle size distribution changes is included because the kernel is updated and explicitly integrated into  $\Gamma_0$  and  $\Gamma_2$  with every time step. This will prove advantageous when additional effects such as sticking are included in the kernel. In addition, source and sink terms need not be parameterized in terms of integer moments and can be implemented directly. An unfortunate disadvantage of this approach is that because the kernel must be integrated (in fact several times) over both  $m$  and  $m'$  every time step to get  $\Gamma_0$  and  $\Gamma_2$ , the CPU time involved is significantly longer than a fully implicit case (e.g., § 2.1; also see § 2.2.2); however, it remains a much faster approach (orders of magnitude) than solving Eq. (1) directly since the cumbersome convolution has been eliminated.

### 2.2.2. Approach 2: Semi-implicit Assumption

Here, we present an alternative moment-based approach to solving the realistic coagulation kernel in which the integer moments appear directly. Unlike the previous case of § 2.2.1, where the double integral of Eq. (5) is used to get the functions of  $m_L$ ,  $\Gamma_0$  and  $\Gamma_2$ , we only integrate over one mass variable (i.e., only integrate one of the integrals), defining the functions

$$C_0(m, t) = \int_{m_0}^{m_L} K(m, m') f(m', t) dm', \quad (24)$$

$$C_2(m, t) = \int_{m_0}^{m_L} m' K(m, m') f(m', t) dm', \quad (25)$$

where the form of the kernel  $K(m, m')$  is the same that in § 2.2.1. We then fit  $C_0$  and  $C_2$  with a finite series in fractional powers of  $m$  in the same manner as given in Eq. (15).

Substituting these functions in place of one of the integrals (say over  $m'$ ), we may integrate over  $m$  to get

$$\begin{aligned} \frac{dM'_0}{dt} &= -\frac{1}{2M_0(0)} \int_{m_0}^{m_L(t)} f(m, t) C_0(m, t) dm = -\frac{1}{2} \sum_i a_i \mu_{p_i} M'_{p_i} \\ \frac{dM'_2}{dt} &= \frac{1}{M_2(0)} \int_{m_0}^{m_L(t)} m f(m, t) C_2(m, t) dm = \sum_i b_i \nu_{p_i+1} M'_{p_i+1}, \\ M'_{p_i} &= [M'_0]^{\frac{1}{2}(p_i-1)(p_i-2)} [M'_1]^{-p_i(p_i-2)} [M'_2]^{\frac{1}{2}p_i(p_i-1)}, \end{aligned} \quad (26)$$

where we have made use of equations (8) and (9) to express the solution in terms of the integer moments  $k = 0, 1, 2$ . Here,  $\mu_{p_i} = M_{p_i}(0)/M_0(0)$ ,  $\nu_{p_i+1} = M_{p_i+1}(0)/M_2(0)$ ,  $M'_k = M_k(t)/M_k(0)$ , and  $0 \leq p_i \leq 1$ . The  $C_k$  are fairly smooth functions over a large range of particle radii; however, the accuracy of fitting a single series in fractional moments over a very broad range of particle sizes (i.e., over many orders of magnitude) may drop off significantly as the broadness of the range increases. This issue may be circumvented by employing a piecewise fit to the integrated kernels  $C_k$ .

It is interesting to note that by this definition of  $C_k$ , we have effectively accomplished what we set out to do in our discussion at the beginning of § 2.2, that is, defining the coagulation kernel in terms of finite series in powers of the mass  $m$ . The difference here is that we have done so through the first integral of the kernel, and not the kernel itself. This means that the mass distribution  $f(m, t)$  is expressed in the calculation of the  $C_k$ , but remains implicit in the definition of the ODEs (Eq. 26). Thus, the method is semi-implicit, because the RHS of the equations above can be expressed in terms of the moments (as defined in Eq. 2). Equations (26) are then integrated using the fourth order Runge-Kutta method, and may be compared with the results of § 2.2.1 and the direct integration of Eq. (1).

This semi-implicit approach tracks the evolving kernel through the integration of Equations (24) and (25) after every timestep, thus the computational time involved is similar to the explicit case. In order to update the kernel, one may solve for the new  $m_L$  after each  $\Delta t$  using the equation ( $q \neq 1$ )

$$\frac{m_L - m_0}{m_L^{2-q} - m_0^{2-q}} - \frac{M_q}{(2-q)M_1} \simeq 0. \quad (27)$$

The new normalization coefficient  $c$  can then be found from the definition of  $M_1 = \rho$ . We then reintegrate Equations (24) and (25) under the powerlaw assumption, and then proceed

to fit the  $C_k(m, t)$  with a finite series in fractional powers of  $m$ . Although, in principle, any other two moments could be used to obtain  $m_L$ ,  $M_q$ , which lies between  $M_2$  and  $M_1$ , and because it roughly characterizes the evolution of the largest particle (see discussion at the end of § 2.2), seems the most consistent choice. The  $q$ -th moment is calculated using the Lagrange polynomial interpolation scheme (Eqs. 8 and 9).

The advantage of the moments method lies in the ability to express the differential equations in terms of the moments of the distribution (i.e., their integrated properties). If a more explicitly mass-dependent approach is adopted (as is the case in § 2.2.1, and the semi-implicit approach described here), then the computational time significantly increases. One can improve the speed of computation by calculating the  $C_k$  periodically, or in the extreme case, only at  $t = 0$  which would make the approach truly *implicit* (e.g., § 2.1). The advantage of an implicit approach is that it becomes fully general (the form of  $f$  is only assumed at the onset), and also in the time it takes to solve ( $< 1$  minute). The bulk of the time is spent in the integration of equations (24) and (25) which would occur only once. The disadvantage, of course, is that the particle velocity distribution is not updated as it changes with time (due to, e.g., changes in the bounds of the size distribution). We present examples of both extremes in § 3.

If one wanted to implement a mass- or velocity-dependent sticking coefficient  $S$ , it can readily be included in the integration to obtain the  $C_k$ . The additional inclusion of source and sink terms due to erosion, fragmentation, or gravitational growth in this semi-implicit formalism would require that we fit these terms in a similar manner to the  $C_k$  so that their subsequent integration over all  $m$  will yield sums over integer moments weighted by different sets of coefficients. Caution must be exercised in fitting, e.g., the gravitational growth term to ensure that the system of equations remains closed. Under such circumstances, a fully explicit approach such as that of § 2.2.1 may be preferred. Alternatively, these effects may be included in particle-histogram space in between coagulation iterations.

Finally, we should point out that allowing for other parameters (such as the index of the powerlaw  $q$ ) to vary with time, does not pose a problem in either of the approaches we have presented. In both cases, one would simply need an additional moment, e.g.  $M_3$ , to determine  $q(t)$ . Similarly, a bifurcated distribution in which the powerlaw exponent changes at a particular particle size (see, e.g., Kenyon & Luu 1999) may also be studied.

In § 3, we will compare the two approaches to the direct integration of the coagulation equation for cases in which there are only systematic velocities ( $v_T = 0$ ), as well as cases in which the velocity differences are induced by turbulent motions.

### 3. Numerical Results

We carried out several calculations in order to demonstrate the accuracy of each alternative method compared to the brute force integration of the collisional coagulation equation. For the purposes of comparison, unless otherwise noted, we chose the initial conditions to be a minimum mass solar nebula at 1 AU at a height of  $z = 10^3$  km above the midplane, and a particle size distribution with a minimum initial radius of 1 cm and a maximum initial radius of 10 cm. The powerlaw exponent  $q = 11/6$ , which is assumed to be constant in these calculations, is representative of a fragmentation population. Standard integrations were carried out with a timestep of  $\Delta t = 10$  years.

#### 3.1. Laminar Case ( $v_T = 0$ )

In Figure 2, we compare the case in which there are only systematic (pressure-gradient driven) velocities between particles ( $v_T = 0$ ). The solid curves represent the explicit assumption (invariant powerlaw slope  $q$  assumed in integration of Equations 22 and 23), while the dashed curves represent the implicit assumption. That is, in the integration of Eq. 26, the form of the mass distribution  $f$  is assumed only at  $t = 0$ . As before, the symbols represent the brute force calculation for two different grid resolutions (solid = 100 bins, open = 1000 bins). Since with the explicit assumption we do not solve for the moments specifically, the values for the solid curves were obtained by substituting the time integrated values of  $c(t)$  and  $m_L(t)$  back into Eq. (17) for  $k = 0, 2$  only. This is because although we have used the moment equations to obtain these results, the explicit assumption of an invariant powerlaw size distribution means that only the equations for the moments  $M_0, M_2$  are needed (although see § 3.2). This is not true, however, for the implicit (and semi-implicit) assumption, where all the moments  $M_0, M_1, M_2$  appear in the differential equations.

We see that there is excellent agreement between both approaches and the numerical values obtained with the highest resolution case. In fact, the agreement between the explicit and implicit assumptions is also quite good. However, at this stage there has not been a great deal of growth (the largest particle size in the distribution has only grown to  $r_L = 11$  cm in size by the end of the simulation for the explicit case). Note that even though in the implicit case the  $C_k$  are calculated only once, the estimate for the largest mass  $m_L$  for the evolving distribution  $f(m, t)$  is still calculated using Eq. (27). At least in the case of minimal or slow growth, it appears that an implicit approach, or even periodic calculation of the  $C_k$ , may be sufficient.

Numerical glitches in the low resolution brute force case arise from the interpolation



scheme for sampling the kernel. In particular, these glitches are likely enhanced because the systematic relative velocities quickly approach zero for identical particle sizes (with the effect much more prominent for larger particles, hence not appearing so much in  $M_0$ ). The higher resolution case contains enough points to smooth out this effect.

Note that (in all simulations) the direct integration of the coagulation equation gives a constant  $M_1$  as is to be expected given that we found  $dM_1/dt = 0$  in the derivation of the moment equations in the absence of sources and sinks; this further validates the numerics of the brute force solution even for the complicated collisional kernel being utilized, and also provides a posteriori validation of our result that  $M_1 = \text{constant}$  from, e.g., Eq. (5), which further validates derivation of equations (24) and (25) which was based on symmetry of the kernel.

### 3.2. Turbulence Case ( $v_T \neq 0$ )

Next, we explored cases in which the systematic velocities were set to zero so that velocity differences between particles are due only to those induced by turbulence. Depending on the magnitude of the turbulence parameter  $\alpha$ , these induced velocities can be either large or small relative to the systematic velocities. To demonstrate, we ran cases for three different values  $\alpha = 10^{-6}, 10^{-5}$ , and  $10^{-4}$ . In the absence of any mechanism to counter growth (e.g., fragmentation), larger  $\alpha$  translates to faster rates of growth (due to larger relative velocities).

In Figure 3 we plot the results for  $\alpha = 10^{-4}$ , for the explicit (solid curves) and implicit (short dashed curves) approaches. The growth rate is more rapid than in the laminar case, with the second scaled moment  $\sim 70\%$  larger (compared to Fig. 2) at the end of the run, meaning that the largest particle size achieved is  $r_L \sim 13.5$  cm. We note that, as was the case for the  $M'_2$  curves in Fig. 2, the explicit and implicit cases are very similar; however, this is not the case for the  $M'_0$  curves. The explicit approach overestimates the value of  $M'_0$  compared to the highest resolution brute force calculation, whereas the implicit approach significantly underestimates the zeroth moment. Both approaches underestimate the value of  $M'_2$ . When we compare integrations of  $M'_2$  for smaller values of  $\alpha$  as we do in Figure 4, we find that both approaches fit the coagulation calculation quite well. The growth rate for these two values of  $\alpha$  are more in line with growth rate found when there are only systematic velocities, so the agreement should not be surprising.

The long-dashed curves in Figures 3 and 4 are the implementation of the semi-implicit approach (§ 2.2.2) in which the  $C_k$  are updated at every time step. In this case, the semi-implicit approach provides a much a much better fit to the brute force calculation, indicating

that the kernel is evolving fast enough that an implicit approach cannot capture this effect. We consider the slight discrepancies between the semi-implicit approach and the brute force calculation to be as much a result of grid resolution as inaccuracy in using the Lagrange polynomial fits to the fractional moments. The explicit and fully implicit approach values of  $r_L$  apparently underestimate the largest particle size relative to the semi-implicit approach (which gives a value of  $r_L \simeq 14$  cm).

Finally, we explored a variation of the explicit approach in which the condition  $M_1 = \rho$  was strictly enforced (recall that  $M_1$  does not appear in Equations 18-19). This amounts to replacing Eq. (18) (derived for  $M_0$ ) with the corresponding equation for  $M_1$ . As a result, we cannot simultaneously fit both  $M_2$  and  $M_0$ . Alternatively, we can use only Eq. (19) for the second moment, by substituting  $c = (2 - q)\rho / (m_L^{2-q} - m_0^{2-q})$  (from the definition of  $M_1$ , Eq. 17) in Eq. (19) so that Eq. (19) alone determines the growth of the largest particle. The differential equation for  $m_L$  then becomes

$$\frac{dm_L}{dt} = \left[ \frac{(3 - q)(2 - q)\rho\Gamma_2}{(3 - q)(m_L^{2-q} - m_0^{2-q})m_L^{2-q} - (2 - q)(m_L^{3-q} - m_0^{3-q})m_L^{1-q}} \right]. \quad (28)$$

The results of the integration of Eq. (28) are shown as the dotted curves in Figure 3 and for the  $\alpha = 10^{-4}$  case in Figure 4. It is clear that this modification provides a much better fit to  $M_2$ , perhaps even better than the semi-implicit case above. However, using  $m_L(t)$  calculated from Eq. (28), and solving for  $c(t)$  does a poor job fitting  $M_0$  (see Figure 3). Thus we conclude that although the modification of the explicit approach matches the brute force calculation of  $M_2$  quite well, only the semi-implicit case is able to provide a simultaneous fit to both the zeroth and second moments (under the condition that  $M_1 = \rho = \text{constant}$ ).

### 3.3. A Model Comparison

Garaud (2007) has developed a simplified analytical approach for dealing with the growth of particles in a turbulent regime, in which the particle size distribution is parameterized by a powerlaw in particle mass with the same exponent we have used in this paper ( $q = 11/6$ ). Similar to what we have presented in previous sections, the underlying assumption of Garaud (2007) is that collisions between particles occur frequently enough that a steady-state balance is reached in the form of the particle size distribution, but with an upper size cutoff that varies with time. Thus, the model of Garaud (2007) is *explicit* and follows only two parameters: the growth of the largest particle  $m_L(t)$ , and the normalization factor  $c(m_L, t)$ .

Given the similarity of the underlying assumptions for the Garaud model and the examples we have presented, it is a useful exercise to compare the results of the two approaches directly. The growth of the largest particle  $r_L$  in the Garaud model (her Eq. 36), expressed in terms of the notation used in this paper, is given by

$$\frac{dr_L}{dt} = \frac{\rho\Omega H}{\rho_s} \sqrt{\frac{\alpha\gamma\text{St}_L}{1 + 64\text{St}_L^2(2 + 5\text{St}_L^{-0.1})^{-2}}}. \quad (29)$$

In Eq. (29)  $\text{St}_L$  is the Stokes number for the largest particle  $r_L = (3m_L/4\pi\rho_s)^{1/3}$ ,  $H = c_g/\Omega$  is the scale height of the gas,  $\gamma$  is the adiabatic index of the gas, and in this expression it is assumed that the sticking coefficient  $S = 1$ , and that  $m_L \gg m_0$ . The above equation is similar to the formula for grain growth proposed by Stepinski & Valageas (1997) to factors of order unity. Finally, we point out that the Garaud model for particle growth is restricted to the value  $q = 11/6$  in order to preserve its completely analytical nature. As a means of a fair comparison, we chose to compare the Garaud model to our explicit case (Eq. 28) for reasons explained below. In the limit of  $m_L \gg m_0$  and  $q = 11/6$ , Eq. (28) becomes

$$\frac{dr_L}{dt} \simeq 0.05 \frac{\rho}{\rho_s} \frac{\Gamma_2}{m_L}. \quad (30)$$

We present the results of our comparison in Figure 5 for the same initial conditions as described at the beginning of § 3.2 (upper curves). We find quite generally that our explicit calculation (Eqs. 28 and 30) leads to a faster growth rate than what is predicted from the Garaud model, initially. We note that the Garaud expression steepens quickly for  $r_L \gtrsim 13$  cm, suggesting that the growth rates of the two approaches are more comparable at later times. However, the minor “kink” in the long-dashed curve is due to the shift from Epstein to Stokes flow. A much more subdued kink is visible in the explicit approach which uses the full expressions for the turbulent velocity, whereas in the derivation of Eq. (29), it is assumed that the stopping time in the Stokes regime is defined by some mean characteristic velocity which leads to a much more noticeable discontinuity. Regardless, the overall more subdued growth rate elicited by Eq. (29) (despite the steepening at later times due to a shift in flow regimes) is apparent from the lower set of curves in Fig. 5 where the initial conditions were chosen with  $r_L(0) = 1$  cm. For this case, growth occurs only in the Epstein regime, but still, the curves for the explicit approach and that calculated from Eq. (29) begin to diverge. Thus, the Garaud expression apparently underestimates the growth rate relative to our approach.

We emphasize that the treatment of particle growth by Garaud (2007) requires several approximations in order to derive a purely analytical expressions for  $dr_L/dt$ . Besides the

aforementioned restriction of  $q = 11/6$ , Garaud approximates the full expressions for the turbulent velocities that we use here by partitioning  $v_T$  into separate cases dependent on the particles’ stopping time relative to the turnover times of the smallest and largest scale eddies. Furthermore, some question may be raised as to the comparability of the moment equations used here to derive Eq. (28), versus the particle growth equation used by Garaud (2007, her Eq. 29). The equation used by Garaud (2007) is more akin to a “sweep-up” equation, with no sources or sinks, than to a formal coagulation equation. Because it bears some resemblance to the equation for  $M_2$  (with some algebra, to factors of order unity), we concluded that our Eq. (28) is the appropriate analog. Despite the differences in growth rate, we find the agreement in the general trend of growth of the two approaches reassuring.

#### 4. Opacity Calculations

Evolutionary models of protoplanetary nebulae, giant planet atmospheres, etc. must somehow treat the escape of thermal radiation (Pollack et al. 1996; Hubickyj et al. 2005; Durisen et al. 2007). In most cases, particles provide the primary opacity for these models. Observations of these and similar objects often rely on Spectral Energy Distributions (SEDs) which can be compared to a model once the model’s internal temperature distribution is known; clear evidence is seen for grain growth in many cases (see review by Natta et al. 2007). Because of the nearly insurmountable computational burden involved with performing a fully self-consistent calculation of particle growth by coagulation along with an already difficult fluid dynamical calculation, most modelers simply assume some invariant particle size distribution, such as the MRN interstellar grain distribution, or make arbitrary assumptions about particle growth (Hubickyj et al. 2005).

In the simplest regime (monodisperse particle radius  $r$  larger than a wavelength), the particle opacity can be written as the area per unit mass:

$$\kappa = \frac{3}{4\rho_s r} \text{ cm}^2 \text{ g}^{-1}; \tag{31}$$

thus growth in radius from  $0.1\mu$  to 1 mm leads to a factor of  $10^4$  change in opacity. To the degree that this wavelength-independent regime holds, including particle size evolution by the moments method in one’s evolutionary models would allow a very simple way to track particle growth and decreasing opacity. For instance, equation (31) above is easily generalized to the area per unit mass integrated over the size distribution:

$$\kappa = \frac{\int \pi r^2 f(m) dm}{\int m f(m) dm} = \left( \frac{9\pi}{16\rho_s^2} \right)^{1/3} \frac{M_{2/3}}{M_1}. \quad (32)$$

As an application of the moments method in Figure 6, we have calculated the decrease in opacity (given by Eq. 32) with time using the semi-implicit approach. An initial particle size distribution with a lower bound of  $r_0 = 0.1$  cm and  $q = 11/6$  was used. Both the pressure gradient driven systematic velocities and the turbulence-induced velocities were used. In the absence of any mechanism to hinder particle growth, larger values of  $\alpha$  lead to more steeply decreasing opacities with time.

In a regime where the particle extinction efficiency  $Q(r, \lambda)$  is wavelength-dependent (say, if the particles are comparable to or smaller than the wavelength), one simply integrates  $Q(r, \lambda)$  over the powerlaw mass distributions resulting from the moments model. For example,

$$\begin{aligned} \kappa_\lambda &= \frac{\int_{m_0}^{m_L} \pi r^2 Q(r, \lambda) f(m) dm}{\int_0^{m_L} m f(m) dm} = \frac{1}{M_1} \int_{m_0}^{m_L} \pi r^2 Q(r, \lambda) c(m_L) m^{-q} dm \\ &= \frac{c(m_L)}{M_1} \left( \frac{9\pi}{16\rho_s^2} \right)^{1/3} \int_{m_0}^{m_L} Q(r, \lambda) m^{2/3-q} dm. \end{aligned} \quad (33)$$

These opacities  $\kappa_\lambda$  can be used to calculate Planck or Rosseland (wavelength-averaged) means for use in radiative transfer models. Recall that the powerlaw slope  $q$  can be freely adjusted within a small but plausible range to explore different growth regimes.

## 5. Porosity

Fractal growth of particles by low-velocity sticking of small solid monomers with radius  $r_o$  and mass  $m_o$  (and/or aggregates of such monomers) causes them to have a density much less than the material density of the monomers (Beckwith et al. 2000; Dominik et al. 2007; Ormel et al. 2008). These porous particles can be described as fractals with dimension  $D$ , such that the particle mass  $m$  increases proportionally to  $r^D$  where  $r$  is some effective radius and  $D$  is the fractal dimension. Thus the particle's internal density is a function of particle size:

$$\rho(r) = \frac{3m}{4\pi r^3} \sim \frac{3m_o(r/r_o)^D}{4\pi r^3} = \frac{3m_o}{4\pi r_o^3} (r/r_o)^{D-3} = \frac{3\rho_o}{4\pi} (r/r_o)^{D-3}. \quad (34)$$

For a typical situation where  $D \sim 2$  (Dominik et al. 2007),  $\rho(r) \propto r^{-1}$  and thus the product  $r\rho(r)$  is a constant across a wide range of particle sizes (until compaction sets in). These more complex but quite plausible particle density-size relationships complicate the expressions for particle stopping time and Stokes number (§ 2.2, Eq. 11; also, see appendix).

Because the particle stopping times enter in through the collisional kernel, the fractal nature of particles can be accounted for using the method of moments in a straightforward manner while maintaining the criterion for closure of the system. We can verify this by noting that the mutual particle cross section

$$\sigma(m, m') = \frac{\pi r_o^2}{m_o^{2/D}} (m^{1/D} + m'^{1/D})^2, \quad (35)$$

is proportional to  $m^{2/D}$ , whereas the stopping time (Eq. 11) in the Epstein regime (the regime that would apply to fluffy fractal aggregates) where the drag force  $F_D = (4/3)\pi r^2 c_g \rho_g \Delta V_{pg}$  (e.g., Cuzzi et al. 1993) is given by

$$t_s = \frac{3m}{4\pi r^2 c_g \rho_g} = \frac{3m_o^{2/D}}{4\pi r_o^2 c_g \rho_g} m^{1-2/D}. \quad (36)$$

In the limit of small Stokes number ( $St \ll 1$ ), both the systematic and turbulence-induced velocities are proportional to  $St$ , so that  $\Delta V \propto t_s \propto m^{1-2/D}$ , and the entire kernel is proportional to  $m$ . For larger  $St$ , the kernel has a shallower powerlaw dependence. Thus, in general, the dependence of  $K(m, m')$  on the mass is  $\lesssim m$ , preserving closure of the system, even for fractal particles. Even though the variation in the properties of the evolving distribution due to porous particles are incorporated directly into the kernel, and are folded into the integration of the explicit approach, the effects of fractal aggregates can, nonetheless, affect which moments characterize what properties in the semi-implicit (or implicit) approach. For example, the wavelength-independent opacity expressed in Eq. (32) takes the form  $\kappa = (\pi r_o^2 / m_o^{2/D}) M_{2/D} / M_1$ .

It should be noted that the value  $D = 2$  represents a special case in that the particle-to-particle relative velocities in the Epstein regime do not depend on the mass of the fractal particle. Indeed, this would seem to indicate that fractal growth can proceed unabated with the corresponding stopping time of the fluffy aggregate remaining the same as that of a single monomer, which would have a significant effect on other particle properties. In particular, the wavelength-independent opacity for  $D = 2$  is constant. However, impacts will eventually lead to compaction or even fragmentation depending on the relative velocities (e.g., Ormel et al. 2007). Both fractal grains and non-fractal particles in the same mass distribution can be

treated in the explicit approach without any modifications, while a piecewise fit to the integrated kernel  $C_k(m)$  (§ 2.2.2) can be used in order to account for the change in regimes in the semi-implicit approach.

## 6. Conclusions

We have demonstrated an approach to solving the collisional coagulation equation with an arbitrary collisional kernel which should be useful in cases when it is only necessary to keep track of general properties of the distribution. This approach involves solving a finite set of coupled differential equations in terms of the integer moments of the particle size distribution. The number of equations (and thus moments) needed depends on the number of properties being tracked. The advantage of the moments method approach is that it allows for considerable savings in computational time compared to direct integration of the coagulation equation, which requires keeping track of every particle size at every spatial location and timestep.

In this paper we have specifically studied the growth of the largest particle under the assumption that the particle size distribution is a powerlaw; however, the technique can be extended to track other properties of the distribution that may change with time. There are many reasons to believe that a powerlaw size distribution is a natural end-state of particle growth, especially those with equal mass per decade, because they have self-preserving properties (Cuzzi & Weidenschilling 2006). With the assumption of a powerlaw distribution, we have provided two different approaches to solving the moment equations, one explicit in which the powerlaw assumption is enforced rigorously at all times, and a semi-implicit approach in which the kernel is integrated over one of the mass variables as much as once every time step. The latter approach can be made fully implicit by only assuming the form of the mass distribution at  $t = 0$ . These approaches are significantly faster than solutions of the coagulation equation because, in particular, the convolution integral (first term on RHS of Eq. 1) has been eliminated. In realistic evolutionary models, intermediate steps performed in particle “histogram” or “size-distribution” space may be interleaved with moments-based coagulation steps in order to account for, e.g., advective/transport terms.

We have compared these alternate approaches to the brute force integration of the full coagulation equation for cases in which there are only systematic velocities, and cases in which the differences in velocity between particles is induced by turbulence. If the growth rate is gradual, the explicit and implicit approaches match the brute force calculation well (Fig. 2), whereas faster growth rates are more difficult to model (Fig. 3). We find that we are able to use the semi-implicit approach in which the  $C_k$  are updated at every timestep,

and a modification to the explicit approach, in which we solve the equation for  $M_2$  only with the assumption of  $\rho = M_1$  strictly enforced, in order to compensate for the faster growth rates. The modification to the explicit approach is useful if one is not particularly interested in following the evolution of the number density of particles, or other properties which may be described by (fractional) moments  $< 1$  (e.g., see § 4). Our results also suggest that a fully implicit approach is probably most useful under circumstances in which the kernel depends on the mass in a straightforward manner (e.g, the Saffman-Turner kernel, § 2.1).

We have compared the approaches developed in this paper to an alternative model for particle growth in a turbulent nebula (Garaud 2007). We have found that there is fairly good agreement in general, but that the curves diverge as time proceeds. This does not appear to be particle-size dependent, or due to a shift in the flow regime. The Garaud expression (Eq. 29) underestimates the growth rate of the largest particle size relative to our approach by only  $\sim 20 - 30\%$  in our comparison. We note that the advantage of the method of Garaud (2007) is that it is purely analytical; however, preservation of her analytical approach requires, amongst other things, the powerlaw exponent be restricted to  $q = 11/6$ . Our approach has no such restriction on the choice of exponent  $q$ , nor for  $q$  to even be a constant.

As a sample application, we show how the moments method can be used in one’s evolutionary model to track particle growth and opacity. As a specific case, we calculated the change in wavelength-independent opacity with time for an initial particle size distribution with upper and lower bounds of  $0.1 - 1$  cm. Both systematic and turbulent velocities were included. In the absence of any mechanism to counter growth, the opacity decreases sharply for higher choices of the turbulent parameter  $\alpha$ . Extension to cases in which the extinction efficiency is wavelength dependent is straightforward. Such opacities can be used to calculate Planck or Rosseland wavelength-averaged means for use in radiative transfer codes.

Finally, we indicate how porous particles with fractal dimension  $D$  can be accounted for in the moments method. The particle-size density relationships that arise affect the particle stopping times and Stokes number, both of which appear only in the collisional kernel. Thus implementation is straightforward. We can treat mass distributions composed of only fractal grains, or both fractal and non-fractal particles. In either case, relatively little modification is needed in the explicit approach, whereas with the semi-implicit (and implicit) approach, a piecewise fit to the integrated kernel  $C_k$  using the method as described in § 2.2.2 can be used to account for the change in particle growth regime when both types of particles are included.

The computational burden of directly solving the coagulation equation makes it quite prohibitive to explore large regions of parameter space, and thus it serves as the primary bottleneck in evolutionary growth models. The approach demonstrated herein is intended



to obtain robust, quantitative results for disk properties such as particle growth timescales and “typical” particle sizes that may be used in modeling efforts that are focused more on the larger problem of planetesimal formation.

Although we have not included sticking or fragmentation in this paper, we believe that the moment equations (Eq. 5) will remain valid at least up to the fragmentation barrier. This size will depend on the assumed particle strengths and choice of nebula parameters. The treatment of growth up to the fragmentation size is consistent with recent work by Brauer et al. (2008) for the case in which additional effects such as radial drift are not included. The model as presented in this paper, however, should be useful for the early stages of protoplanetary nebula particle growth relevant to spectral energy distributions and MRI suppression.

In a forthcoming paper we will explore the effects of a variable sticking coefficient  $S(m, m')$ . Furthermore, we will explore the addition of source and sink terms such as gravitational growth, erosion, sublimation, and condensation in addition to fragmentation. The ultimate goal will be to apply this methodology to a global model that studies the evolution of both the gas and solids in nebular and subnebular (giant planetary) environments.

We wish to thank Sandy Davis, Fred Ciesla, and Olenka Hubickyj for internal reviews which improved the exposition of this paper, and an anonymous reviewer for his or her careful analysis of the manuscript. This work was supported by a grant from NASA’s Origins of Planetary Systems Program.

### A. Generalization of the Systematic (Pressure Gradient Driven) Velocities

In this appendix, we generalize the basic equations of Nakagawa et al. (1986, also, see Tanaka et al. 2005) for a two-component fluid by extending the particle component to incorporate a size distribution. We adopt cylindrical coordinates  $(R, \phi, Z)$ , designating the corresponding gas velocity components as  $(u, v, w)$  and the particle velocity components as  $(U_i, V_i, W_i)$ . The equations of motion of particles and gas for the radial and tangential velocities, generalized for a particle size distribution, are given by

$$\frac{\partial U_i}{\partial t} = -A_i \rho_g (U_i - u) + 2\Omega V_i, \tag{A1}$$

$$\frac{\partial V_i}{\partial t} = -A_i \rho_g (V_i - v) - \frac{1}{2}\Omega U_i, \tag{A2}$$

$$\frac{\partial u}{\partial t} = - \sum_j A_j \rho_j (u - U_j) + 2\Omega v - \frac{1}{\rho_g} \frac{\partial p_g}{\partial R}, \quad (\text{A3})$$

$$\frac{\partial v}{\partial t} = - \sum_j A_j \rho_j (v - V_j) - \frac{1}{2} \Omega u, \quad (\text{A4})$$

where the system is assumed to be axysymmetric. Here,  $A_i = (\rho_g t_{si})^{-1}$  with  $t_{si}$  the stopping time of a particle of radius  $r_i$ ,  $\rho_g$  and  $p_g$  are the gas mass density and pressure, and  $\rho_j$  is the material density of particles of radius  $r_j$ . We have not included the vertical component equations; here, generalization to a particle size distribution is straightforward since it remains true in general that  $|w/W_i| \ll 1$ ; that is, the vertical gas component of the velocity  $w$  is negligibly small compared with  $W_i$  (see appendix, Nakagawa et al. 1986).

If the dust stopping time is short compared to the orbital period, we can seek steady-state solutions for the velocity components. Setting  $\partial/\partial t = 0$ , this system can be solved exactly in the Epstein regime. By solving Eq. (A1) for  $V_i$  and inserting into Eq. (A2), we obtain

$$U_i = \frac{A_i^2 \rho_g^2 u + 2\Omega A_i \rho_g v}{A_i^2 \rho_g^2 + \Omega^2} = \frac{u + 2v \text{St}_i}{1 + \text{St}_i^2}, \quad (\text{A5})$$

$$V_i = \frac{-(\Omega/2) A_i \rho_g u + A_i^2 \rho_g^2 v}{A_i^2 \rho_g^2 + \Omega^2} = \frac{v - (1/2)u \text{St}_i}{1 + \text{St}_i^2}, \quad (\text{A6})$$

where  $V_i$  was obtained by insertion of  $U_i$  back into Eq. (A1). In Eqs. (A5)-(A6) we have expressed the last equality in terms of the Stokes number  $\text{St}_i = t_{si} \Omega$ , with  $\Omega$  being the local Kepler frequency. These expressions for the individual particle velocity components can be inserted into Eqs. (A3) and (A4) to yield expressions for radial and tangential gas velocity components. With little difficulty, one finds

$$u = 2\eta v_K \frac{s_1}{s_1^2 + (1 + s_0)^2}, \quad (\text{A7})$$

$$v = -\eta v_K \frac{1 + s_0}{s_1^2 + (1 + s_0)^2}, \quad (\text{A8})$$

where

$$s_0 = \sum_j \frac{A_j^2 \rho_g \rho_j}{A_j^2 \rho_g^2 + \Omega^2} = \sum_j \frac{\rho_j}{\rho_g} \frac{1}{1 + \text{St}_j^2}, \quad (\text{A9})$$

$$s_1 = \Omega \sum_j \frac{A_j \rho_j}{A_j^2 \rho_g^2 + \Omega^2} = \sum_j \frac{\rho_j}{\rho_g} \frac{\text{St}_j}{1 + \text{St}_j^2}. \quad (\text{A10})$$

and  $\eta = -(1/2\rho_g\Omega^2 R)(\partial p_g/\partial R)$ . These expressions agree with those obtained by Tanaka et al. (2005) with the exception that their expressions for  $s_0$  and  $s_1$  are expressed in integral form.

From these expressions, one can easily obtain expressions for the relative velocities with respect to the gas  $U_i - u$  and  $V_i - v$ , or the relative velocities between particles of different sizes  $U_i - U_j$  and  $V_i - V_j$ . These expressions are also applicable for the Stokes regime in which the stopping times are a function of the relative particle-gas velocities (cf. Eq. 11). In this case, iterations must be performed in order to obtain the correct relative velocities. Convergence is generally achieved in a small number of iterations.

## REFERENCES

- Beckwith, S. V. W., & Sargent, A. I. 1991, *ApJ*, 381, 250
- Beckwith, S. V. W., Henning, T., & Nakagawa, Y., In *Protostars and Planets IV*, V. Mannings, A. P. Boss, and S. S. Russell, eds., (Tucson: Univ. of Arizona Press), 533
- Brauer, F., Dullemond, C. P., & Henning, Th., 2008, *A&A*, 480, 859
- Bromley, B. C., & Kenyon, S. J., 2006, *AJ*, 131, 2737
- Cuzzi, J. N., Dobrovolskis, A. R., & Champney, J. M. 1993, *Icarus*, 106, 102
- Cuzzi, J. N., & Hogan, R. C. 2003, *Icarus*, 164, 127
- Cuzzi, J. N., & Weidenschilling, S. J. 2006, In *Meteorites of the Early Solar System II*, D. S. Loretta, and H. Y. McSween, Jr., eds., (Tucson: Univ of Arizona Press), 353
- Dominik, C., Blum, J., Cuzzi, J. N., & Wurm, G. 2007, In *Protostars and Planets V*, B. Reipurth, D. Jewitt, and K. Keil, eds., (Tucson: Univ. of Arizona Press), 783
- Dullemond, C. P., & Dominik, C. 2005, *A&A*, 434, 971
- Durisen, R. H., Boss, A. P., Mayer, L., et al., 2007, In *Protostars and Planets V*, B. Reipurth, D. Jewitt, and K. Keil, eds, (Tucson: Univ of Arizona Press), 607
- Garaud, P, 2007, arXiv:0705.1563, Submitted to *ApJ*

- Hubickyj, O., Bodenheimer, P., & Lissauer, J. J., 2005, *Icarus*, 179, 415
- Johansen, A., Oishi, J. S., Low, M.-M. M., et al. 2007, *Nature*, 448, 1022
- Kessler-Silacci, J., Augereau, J.-C., Dullemond, C. P., et al. 2006, *ApJ*, 639, 275
- Kenyon, S. J., & Luu, J. X., 1999, *ApJ*, 526, 465
- Leinhardt, Z. M., & Richardson, D. C., 2005, *ApJ*, 625, 427
- Loginov, V. I. 1979, *Dehydration and Desalinization of Oil: Khimiya, Moscow*
- Markiewicz, W. J., Mizuno, H., & Völk, H. J. 1991, *A&A*, 242, 286
- Marov, M. Ya., & Kolesnichenko, A. V. 2001, *Mechanics of Turbulence of Multicomponent Gases: Kluwer Academic Publishers*
- Nakagawa, Y., Sekiya, M., & Hayashi, C. 1986, *Icarus*, 67, 375
- Natta, A., Testi, L., Calvet, N., et al., 2007, In *Protostars and Planets V*, B. Reipurth, D. Jewitt, and K. Keil, eds, (Tucson: Univ of Arizona Press), 767
- Ormel, C. W., & Cuzzi, J. N. 2007, *A&A*, 413, 466
- Ormel, C. W., Spaans, M., & Tielens, A. G. G. M. 2007, *A&A*, 461, 215
- Ormel, C. W., Cuzzi, J. N., & Tielens, A. G. G. M. 2008, *A&A*, submitted
- Pollack, J. B., Hubickyj, O., Bodenheimer, P., et al., 1996, *Icarus*, 124, 62
- Press, W. H., Teukolsky, S. A., Vetterling, W. T., & Flannery, B. P. 1992, *Numerical Recipes in Fortran: 2nd edition*, Cambridge University Press.
- Przygodda, F., van Boekel, R., Àbrahàm, P., et al. 2003, *A&A*, 412, L43
- Saffman, P. G., & Turner, J. S., 1956, *J. Fluids Mech.*, 1, 16
- Safronov, V. S. 1969, *Evolution of the Protoplanetary Cloud and the Formation of the Earth and Planets: NASA TTF-677*, 1972
- Silk, J., & Takahashi, T., 1979, *ApJ*, 229, 242
- Smoluchowski, M., 1916, *Phys. Z*, 17, 557
- Stepinski, T. F., & Valageas, P., 1997, *A&A*, 319, 1007

- Tanaka, H., Himeno, Y., & Ida, S., 2005, *ApJ*, 625, 414
- Trubnikov, B. A. 1971, *Soviet Phys. - Doklady*, 16, 124
- van Boekel, R., Waters, L. B. F. M., Dominik, C., et al. 2003, *A&A*, 400, L21
- Völk, H. J., Morfill, G. E., Roeser, S., & Jones, F. C. 1980, *A&A*, 85, 316
- Weidenschilling, S. J., 1977, *MNRAS*, 180, 57
- Weidenschilling, S. J., 1984, *Icarus*, 60, 553
- Weidenschilling, S. J., 1997, *Icarus*, 127, 290
- Weidenschilling, S. J., 2000, *Space Sci. Rev.*, 92, 295
- Weidenschilling, S. J., 2002, *Met.& Pla. Sci.*, 37, A148.
- Weidenschilling, S. J., 2004, In *Comets II*, ed. M. C. Festou, H. U. Keller, & H. A. Weaver (Tucson: Univ. of Arizona Press), 97
- Weidenschilling, S. J., & Cuzzi, J. N. 1993, In *Protostars and Planets III*, ed. E. H. Levy & J. I. Lunine (Tucson: Univ. of Arizona Press), 1031

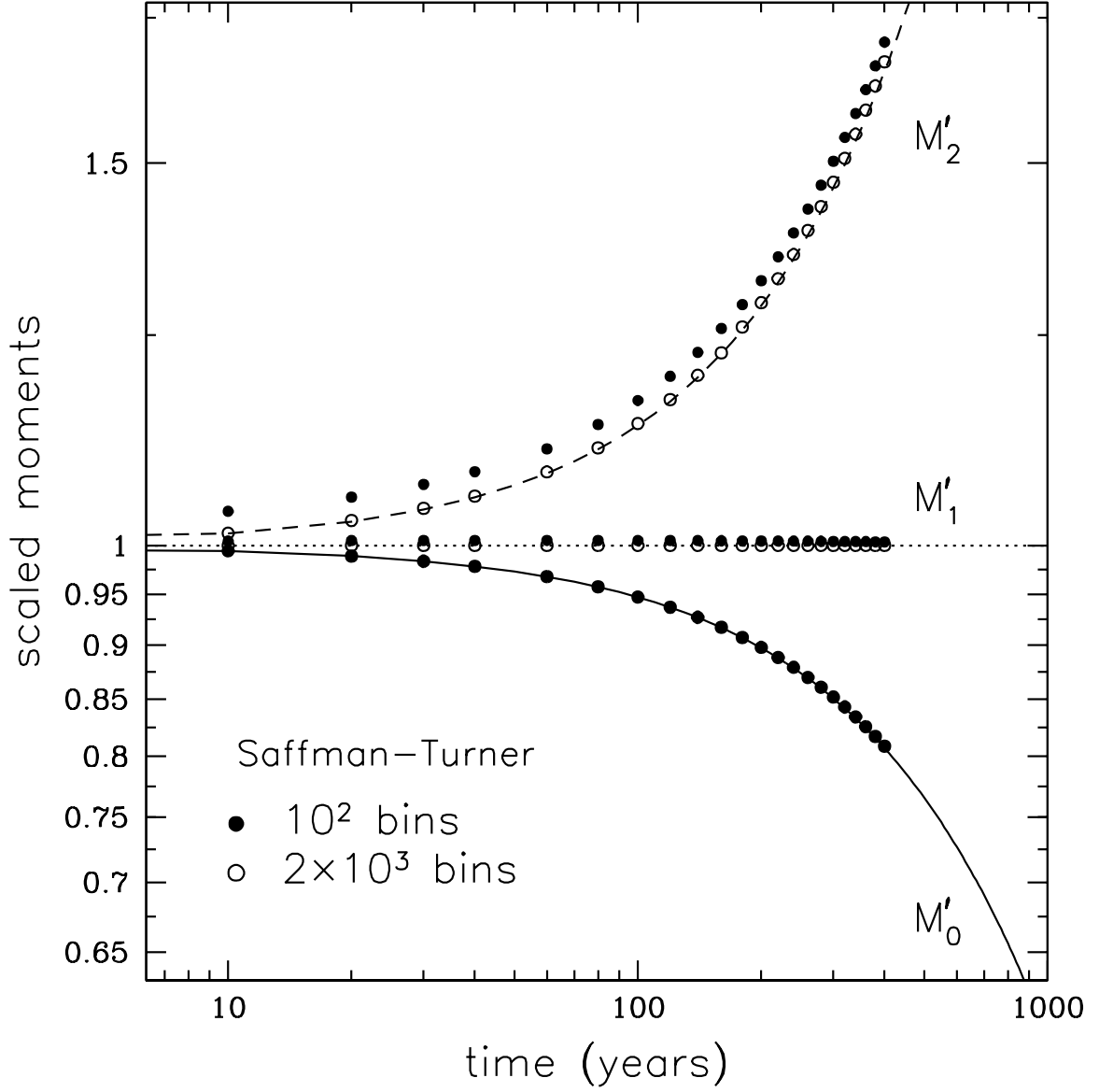


Fig. 1.— Comparison between the scaled integer moments  $M'_k = M_k/M_k(0)$  for  $k = 0, 1, 2$  (curves) obtained by the method of moments calculation with a simple Saffman-Turner turbulent coagulation kernel (Eq. 7) and a brute force integration (symbols) of the coagulation equation (Eq. 1). The integer moments for the latter are calculated a priori using the distribution function  $f(m, t)$ . There is good agreement, especially for the higher resolution case.

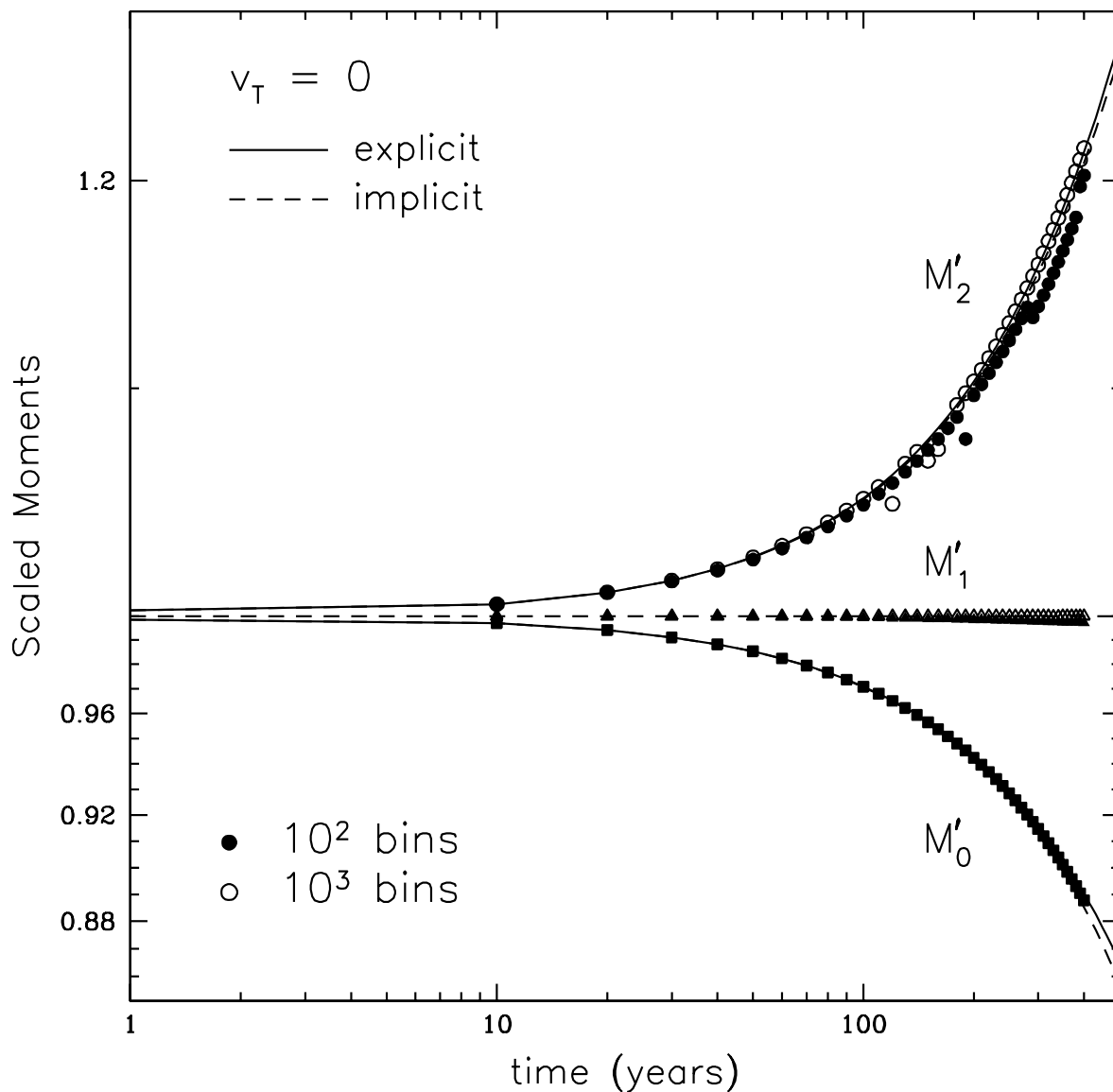


Fig. 2.— Comparison of the scaled integer moments  $k = 0, 1, 2$  obtained from the moments method (curves), and those obtained from the integration of the coagulation equation (Eq. 1, symbols) for the case of a realistic collision kernel with  $v_T = 0$ . Both the explicit (solid curves), and implicit (short-dashed curves) approaches match the coagulation calculation fairly well, especially the higher resolution case.

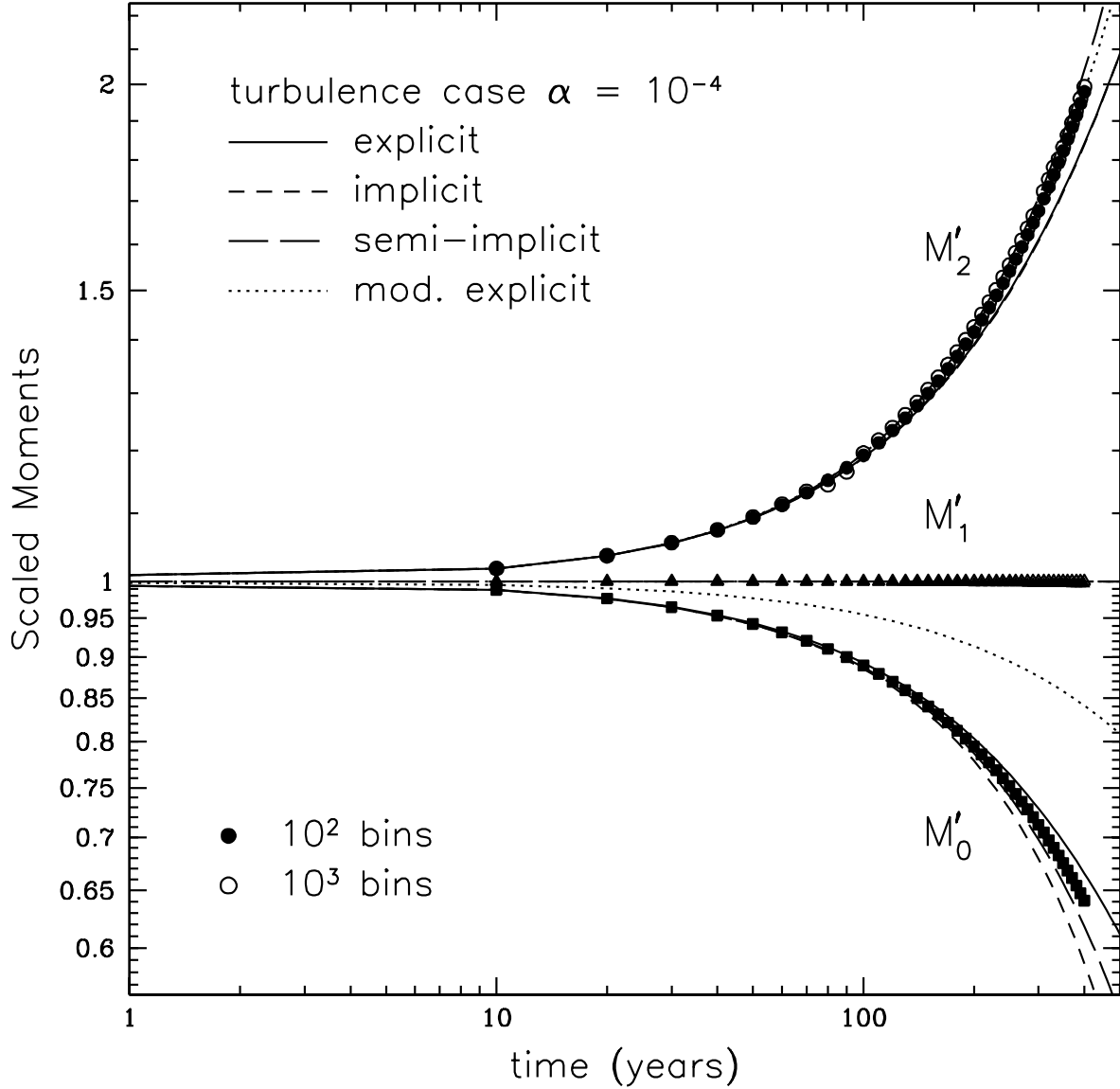


Fig. 3.— Comparison of the scaled integer moments  $M_k$  for  $k = 0, 1, 2$  obtained from the moments method, with results obtained from the brute force integration of the coagulation equation (Eq. 1) for the case of a realistic collision kernel with  $v_T \neq 0$  (and no systematic velocities). In this case the turbulence parameter  $\alpha = 10^{-4}$ . Both the explicit (solid curves) and implicit (short-dashed curves) approaches have some difficulty matching the coagulation calculation for both  $M_0$  and  $M_2$  (note that the solid and short-dashed curves for  $M_2$  lie on top of each other). However, the semi-implicit approach (long-dashed curves) provides a better fit. The modified explicit approach (dotted curves) provides a better fit for  $M_2$  while giving a worse fit for  $M_0$  (see § 3.2).



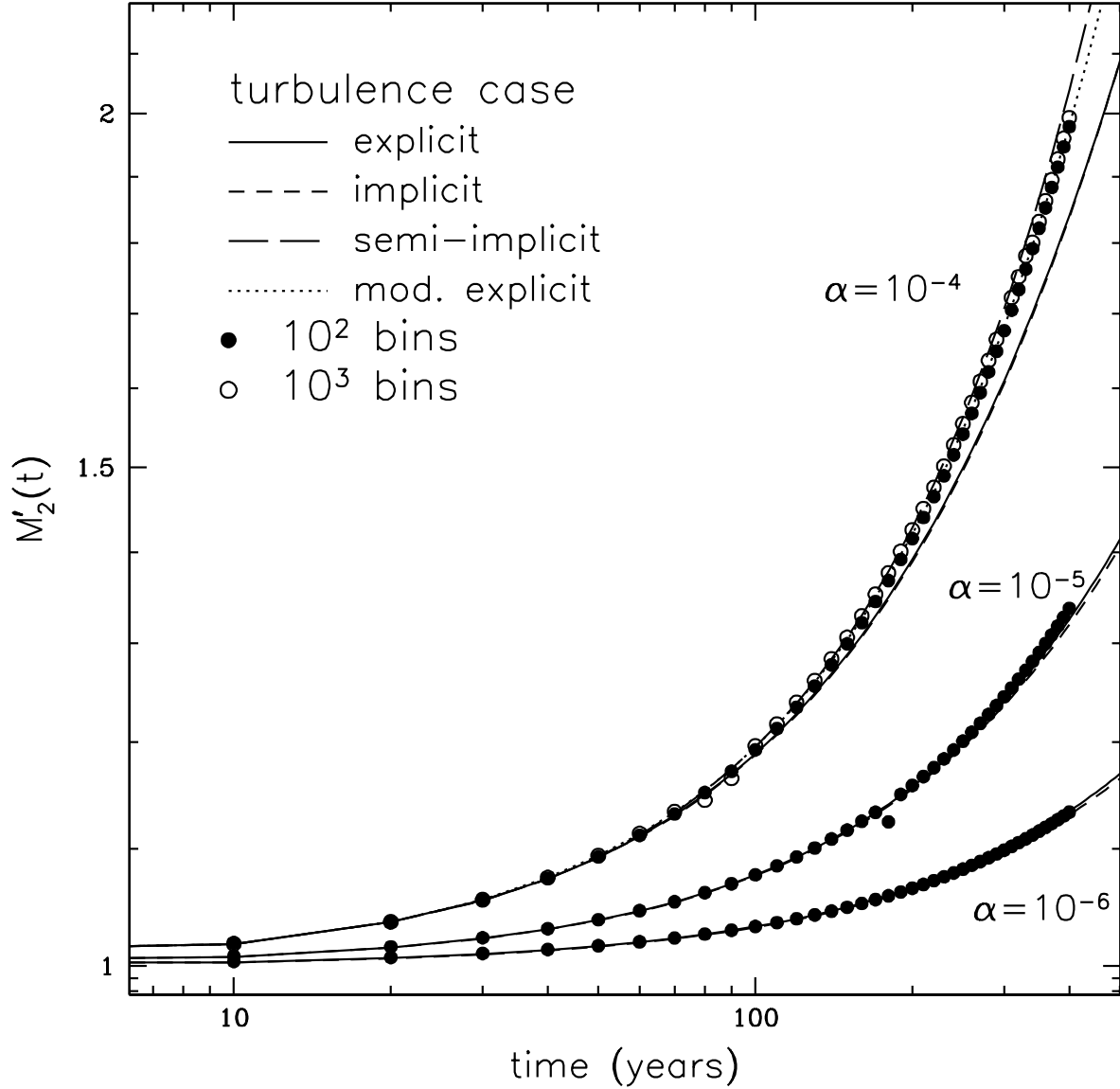


Fig. 4.— Comparison of the second moment  $M'_2(t)$  obtained from the moments method with that obtained from integration of the coagulation equation (Eq. 1) for the case of a realistic collision kernel with  $v_T \neq 0$  (and no systematic velocities) for three different values of the turbulence parameter  $\alpha$ . Both the explicit (solid curves) and implicit (short-dashed curves) approaches match the lower  $\alpha$  values fairly well, but as indicated in fig. 3, have difficulty matching the case of  $\alpha = 10^{-4}$  (note that the solid and short-dashed curves lie on top of each other). However, not surprisingly, the semi-implicit approach (long-dashed curves) and a modified explicit approach (for  $M_2$  only, dotted curve) provides a much better fit (see § 3.2).

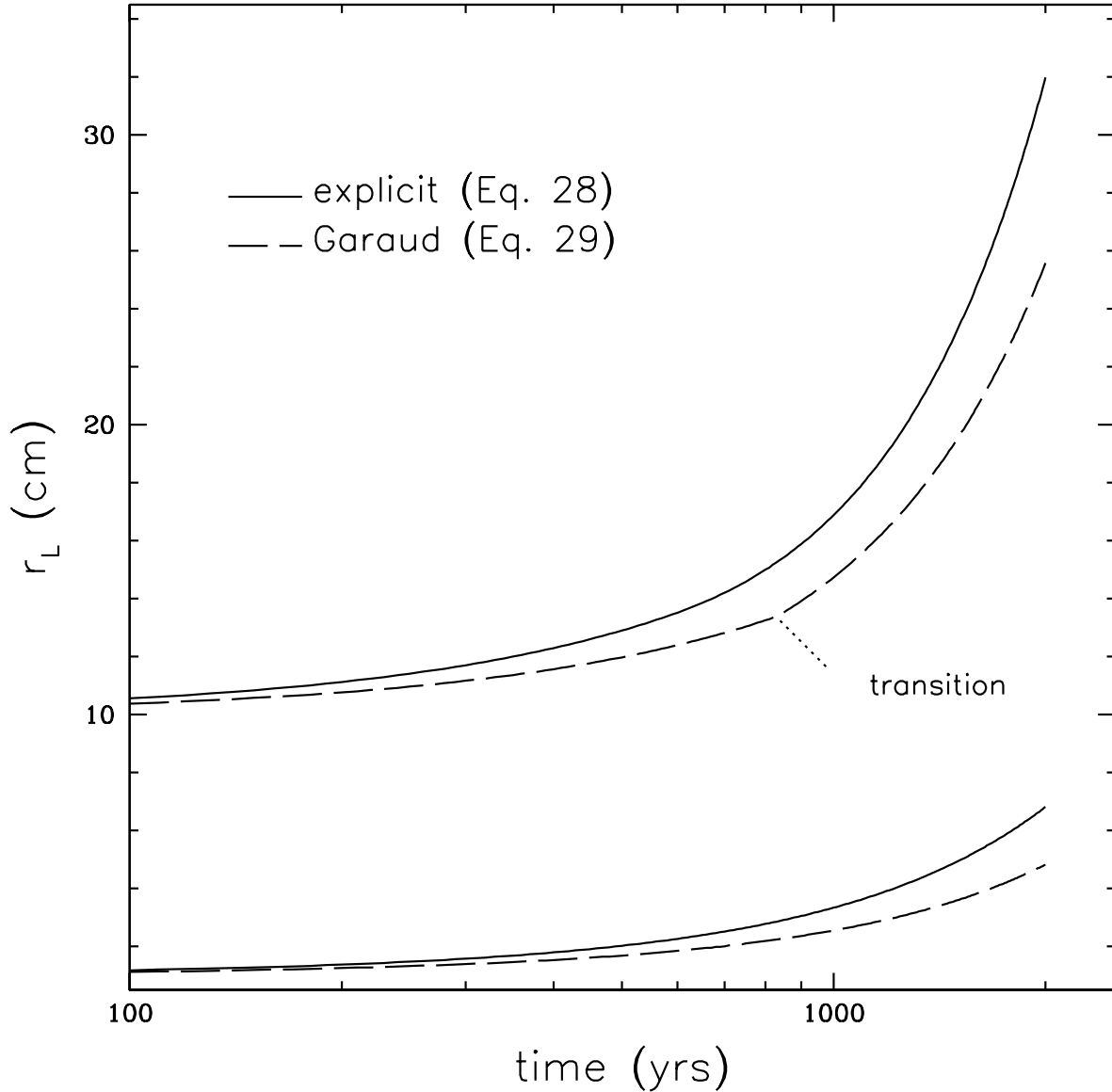


Fig. 5.— Comparison of particle growth as a function of time using the explicit approach (Eq. 28, solid curve), and the Garaud (2007) analytical particle growth expression (long-dashed curve). The upper and lower sets of curves differ in the initial size of the largest particle. Both sets of curves begin to diverge immediately. The somewhat subdued kink in the upper curves at  $r_L \sim 13.5$  cm is due to a shift from Epstein to Stokes flow. However, overall, the agreement is not bad ( $\sim 20 - 30\%$  in  $r_L$ ).

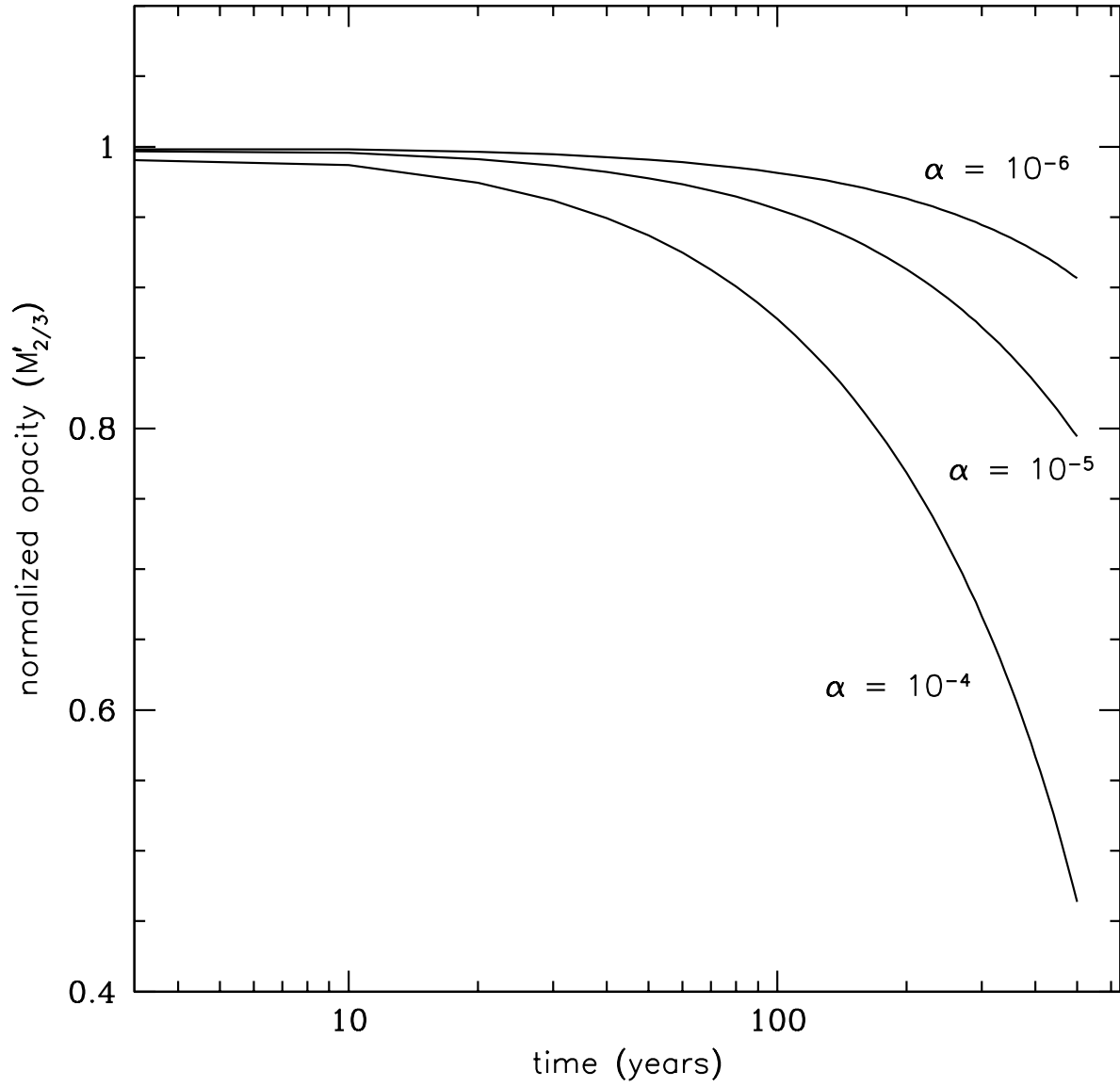


Fig. 6.— Plot of the normalized (to initial value) wavelength-independent opacities for different choices of the turbulence parameter  $\alpha$ . Opacities decrease sharply (in the absence of any mechanism to hinder particle growth) for higher  $\alpha$ . Calculations were performed using the semi-implicit approach with both turbulent and systematic relative velocities included.